MHD Wave Modes Resolved in Fine-Scale Chromospheric Magnetic Structures

Verth, G., & Jess, D. B. (2016). MHD Wave Modes Resolved in Fine-Scale Chromospheric Magnetic Structures. In A. Keiling, D-H. Lee, & V. Nakariakov (Eds.), Low-Frequency Waves in Space Plasmas. (pp. 433-448). (Geophysical Monograph Series). John Wiley & Sons, Inc. DOI: 10.1002/9781119055006.ch25

Published in:
Low-Frequency Waves in Space Plasmas

Document Version:
Publisher's PDF, also known as Version of record

Section X
Solar Photosphere and Chromosphere

25

MHD Wave Modes Resolved in Fine-Scale Chromospheric Magnetic Structures

G. Verth[1] and D. B. Jess[2]

25.1. INTRODUCTION

Due to its complex and dynamic fine-scale structure, the chromosphere is a particularly challenging region of the Sun's atmosphere to understand [e.g., see *Judge*, 2006]. It is now widely accepted that to model chromospheric dynamics, even on a magnetohydrodynamic (MHD) scale, while also calculating spectral line emission, one must realistically include the effects of partial ionization and radiative transfer in a multi-fluid plasma under non-LTE conditions [e.g., *Hansteen et al.*, 2007]. Within the past decade there has been a concerted international effort to try and advance our understanding of this tantalizing layer of the solar atmosphere, which is thought to be a key part of solving the solar atmospheric heating problem. There have certainly been major advances in chromospheric observations from high-spatial and temporal resolution space-borne and ground-based instruments. These include Hinode [*Kosugi et al.*, 2007] launched in 2006 and the Rapid Oscillations in the Solar Atmosphere (ROSA) [*Jess et al.*, 2010a] multi-wavelength camera system based at the Dunn Solar Telescope (DST), which became operational in 2009. Furthermore, in 2013, the Interface Region Imaging Spectrograph (IRIS) [*De Pontieu et al.*, 2014] was launched with the specific task of studying in unprecedented detail the previously little explored UV lines formed in the interface region between the chromosphere and corona.

There now seems to be general agreement that the Sun's magnetic field is primarily responsible for plasma heating in its atmosphere, from the photosphere up through the chromosphere, interface region, and finally into the corona. However, a rigorous debate is ongoing as to which plasma processes are actually responsible. Historically, popular proposed mechanisms such as MHD wave dissipation or magnetic reconnection have had little direct observational evidence to support them due to the small spatial scales involved and the limited resolution of past instrumentation. For example, earlier space-borne EUV and X-ray wavelength instruments launched in the 1990s, with their limited spatial and/or temporal resolutions, such as the SOlar and Heliospheric Observatory (SOHO) [*Domingo et al.*, 1995] and the Transition Region and Coronal Explorer (TRACE) [*Handy et al.*, 1999], could only detect less frequent high-energy reconnection/wave events. However, it is now apparent that most of the heating in the solar atmosphere is taking place on small spatial scales, certainly less than ~100 km perpendicular to the magnetic field direction. As a result the rarity of large-scale reconnection/wave events related to, for example, flares and CMEs means that these do not play a key role.

Regarding the chromosphere, since it can be observed from ground-based telescopes with much higher spatial and temporal resolutions than are currently possible for the corona, it has presented an opportunity to study the small-scale and ever-present dynamics of thin ($\lesssim$1000 km wide) chromospheric magnetic features such as spicules, fibrils, and mottles. These are particularly visible in narrowband spectral filters such as H α and Ca II H and K, which have aided tremendously in the

[1]*Solar Physics and Space Plasma Research Centre (SP²RC), The University of Sheffield, Sheffield, UK*

[2]*Astrophysics Research Centre, School of Mathematics and Physics, Queen's University Belfast, Belfast, Northern Ireland, UK*

Low-Frequency Waves in Space Plasmas, Geophysical Monograph 216, First Edition.
Edited by Andreas Keiling, Dong-Hun Lee, and Valery Nakariakov.

identification of various MHD wave modes propagating along such fine-scale chromospheric magnetic structures. Prior to these modern high-resolution chromospheric observations, an abundance of MHD waves was expected to be present in the Sun's lower atmosphere because it is in essence an elastic/compressible medium permeated by strong magnetic fields that are constantly being stressed and perturbed by the magnetoconvective motions generated from below (see Chapter 26 for an overview of photospheric wave modes). In agreement with these expectations, it has now been confirmed that there are indeed both Alfvénic and magnetoacoustic wave modes propagating along chromospheric waveguides at all times [e.g., *De Pontieu et al*., 2007; *He et al*., 2009a, b; *Morton et al*., 2012a; *Kuridze et al*., 2012, 2013].

A significant breakthrough now is that with contemporary multi-instrumental studies we can see how small-scale disturbances generated in the photosphere impact on the higher atmospheric layers. For example, in the particular case of ubiquitous small-scale (≈ 1000 km diameter) photospheric vortical motions, *Wedemeyer-Böhm et al*. [2012] traced the resultant energy transfer of associated magnetic tornadoes up through the atmosphere by exploiting simultaneous photospheric, chromospheric, and coronal observations using the ground-based CRisp Imaging Spectropolarimeter (CRISP) [*Scharmer et al*., 2008] at the Swedish Solar Telescope (SST) and also the Atmospheric Imaging Assembly (AIA) [*Lemen et al*., 2012] onboard the Solar Dynamics Observatory (SDO). SDO, launched in 2010, is especially useful in detecting the coronal signatures of energy propagation from the lower atmosphere because it continually observes the full solar disc, sampling UV/EUV emission about every 10 s. This makes it much easier for observers to compare cospatial/temporal coronal data to photospheric/chromospheric data gathered from specific, limited duration ground-based campaigns.

With all these new possibilities, there has been a step-change in all-encompassing solar atmospheric MHD wave studies in the past decade. Now, in simultaneous multi-wavelength observations, it is possible to observe abundant chromospheric waves, along with their photospheric drivers and associated coronal signatures [e.g., *Morton et al*., 2014]. However, before we can start considering the energetics of the waves and their possible contribution to plasma heating, the very first step that must be taken is to accurately identify which wave modes are being observed. This is not a trivial task and has actually been the cause of much debate since the first wave interpretations of Hinode's chromospheric data [e.g., see *Erdélyi and Fedun*, 2007; *Van Doorsselaere et al*., 2008]. However, without this knowledge, it not possible to quantify what the wave cutoff behavior and most likely damping mechanisms could be. In fact specific MHD wave modes can have different dominant (or competing) frequency-dependent damping mechanisms, such as thermal conduction, radiative cooling, kinematic viscosity, MHD radiation, resonant absorption, and phase mixing [e.g., see *Aschwanden*, 2004]. This can result in wildly varying damping rates for different MHD wave modes and, in turn, their ultimate effectiveness for atmospheric heating. Hence accurate quantification of MHD wave energetics must be founded on a precise identification of the actual wave mode (or combination of wave modes) being observed, as documented in the recent review by *Jess et al*. [2015].

Thus far the benefits of accurate wave mode identification have been threefold; first, they allow us to more precisely quantify the chromospheric energy flux associated with each mode [*Morton et al*., 2012a; V*an Doorsselaere et al*., 2014]; second, the broadband frequency information of MHD waves allows us to study the frequency-dependent wave damping [*Verth et al*., 2010; *Morton et al*., 2014]; third, it allows a complimentary approach to understanding the fine-scale plasma structure of the chromosphere by implementing magnetoseismological techniques [*Fedun et al*., 2011b; *Verth et al*., 2011; *Morton et al*., 2012b; *Kuridze et al*., 2013; *Morton*, 2014]. These are all crucial gains that were only made possible in the last decade due to the launch of Hinode, combined with significant improvements in ground-based spectroscopic/imaging observations (ROSA/DST and CRISP/SST) and polarimetry, notably with the Coronal Multi-channel Polarimeter (CoMP) [*Tomczyk and McIntoch*, 2009]. Subsequent to the launch of SDO and IRIS, there is an urgent need to combine the best cutting-edge observational and modeling studies so that forward leaps in solar physics can be facilitated. This will open a whole new era of studying the heat generated through fine-scale plasma dynamics in the solar atmosphere, not just through the study of waves but also, for example, instabilities and nanoflare heating events.

25.2. MHD KINK-MODE IDENTIFICATION

Although quasi-periodic line widths and Doppler velocities were detected in solar spicule data as far back as the 1960s [e.g., *Nikol'sky and Sazanov*, 1967; *Pasachoff et al*., 1968; *Weart*, 1970], the limited spatial and temporal resolutions of this era prevented the identification of specific MHD wave modes. Spicules have been of much interest to solar physicists for much longer. In fact they were first reported in scientific literature as far back as *Secchi* [1877]. Nowadays they are known to be thin jets of plasma channeled by the magnetic field in the Sun's lower atmosphere (e.g., see the review by *Zaqarashvili and*

Erdélyi [2009]). However, what causes their formation and what their contribution is to plasma heating (if any) is still the matter of fierce debate [e.g., see De *Pontieu et al*., 2011; *Klimchuk*, 2012].

Spicules, which are predominantly rooted at network boundaries, are seen off-limb in a 2D projection as a "thick forest" in chromospheric lines such as H α and Ca II H and K. The first claim of kink wave detection in spicules was by *Kukhianidze et al*. [2006] using Hα Doppler data from the coronagraph and universal spectrograph based at the Abastumani Astrophysical Observatory in Georgia. However, it took high-resolution imaging data from the Solar Optical Telescope (SOT) [*Suematsu et al*., 2008; *Tsuneta et al*., 2008b] onboard Hinode to observe this particular MHD wave mode more unambiguously [*De Pontieu et al*., 2007]. Periodic motions, perpendicular to the direction of the magnetic field, were detected in spicules using the Ca II H filter of SOT (see Figure 25.1). This strongly suggested that the main restoring force for these waves was magnetic tension and led *De Pontieu et al*. [2007], and later *He et al*. [2009a], to simply interpret them as Alfvén waves [*Alfvén*, 1942] with their phase speed, c_A, governed by the well-known relation

$$c_A = \frac{B}{\sqrt{\mu\rho}} \tag{25.1}$$

where B is the magnetic field strength, μ is the magnetic permeability, and ρ is the plasma density. Theorists immediately started debating the validity of this interpretation [e.g., see *Erdélyi and Fedun*, 2007; *Van Doorsselaere et al*., 2008]. The base objection was that Alfvén's linear wave and planar geometry model assumed the plasma to be completely homogeneous, and was therefore not accurate enough to predict the observed properties of waves traveling through the Sun's inhomogeneous and finely structured atmosphere. In fact spicules have a finite width (diameter $\lesssim$1000 km) and likely have a substantial variation in plasma density transverse to the direction of the magnetic field [e.g., *Beckers*, 1968], further fueling the debate as to whether bulk Alfvén waves were the correct interpretation.

Recent 3D MHD radiative transfer simulations suggest that spicules could be formed by a localized and enhanced Lorentz force at their base, which squeezes the chromospheric plasma in such a way that it is thrown up to lower coronal heights [*Martínez-Sykora et al*., 2011, 2013]. Such cutting-edge numerical modeling supports the idea of spicules being overdense relative to the ambient plasma. If one assumes that on average spicules represent thin magnetically dominated filaments of plasma, with chromospheric densities and temperatures that penetrate into the corona, then the observed transverse motions indeed have to be modeled as MHD waves propagating along an

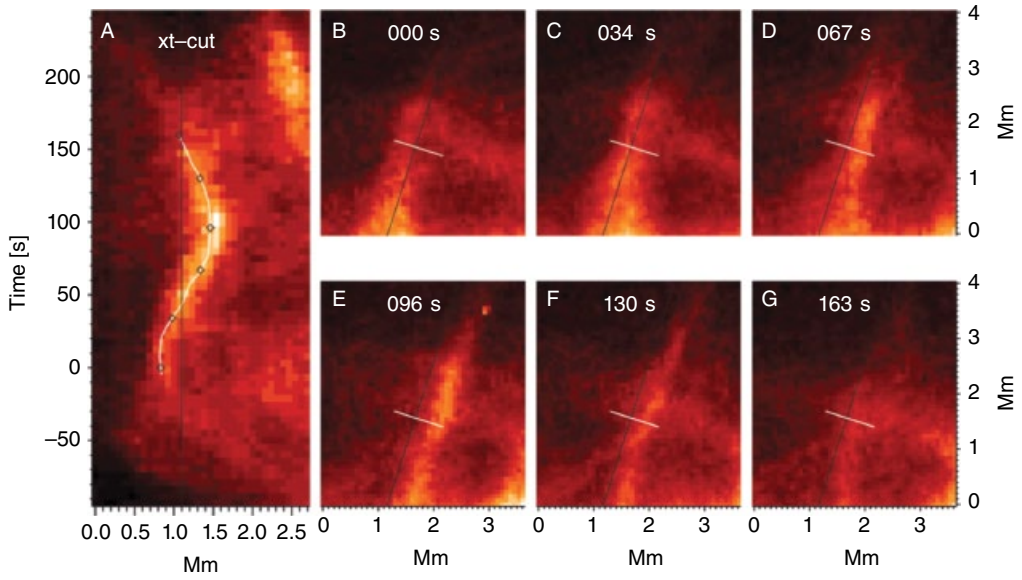

Figure 25.1 Example of an MHD kink wave observed off-limb in a spicule using the Ca II H filter of Hinode/SOT by *De Pontieu et al*. [2007]. The panels demonstrate the plane-of-sky projection of the spicule's motion. The largest (left-hand) panel shows a time–distance diagram taken at a slice approximately perpendicular to the spicule axis. The smaller panels reveal sequential snapshots of the spicule and indicate the perpendicular slice a white line. Image reproduced from *De Pontieu et al*. [2007].

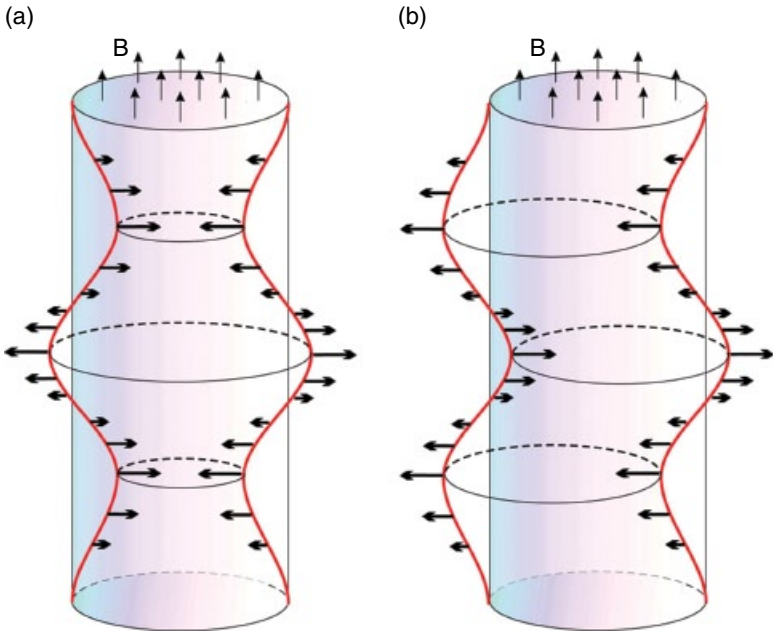

Figure 25.2 Cartoon illustrating the MHD sausage and kink waves in a magnetic flux tube. (a) Sausage wave, which has $m = 0$, characterized by an axisymmetric contraction and expansion of the tube's cross-section. This produces a periodic compression/rarefaction of both the plasma and magnetic field. (b) Kink wave, which has an azimuthal wavenumber $m = 1$. This is notable since it is the only value of m that causes a transverse displacement of the flux tube. Unlike the sausage wave, the kink wave displacement/velocity field is not axisymmetric about the flux tube axis. The red lines show the perturbed flux tube boundary and thick arrows show the corresponding displacement vectors. The thin arrows labeled B show the direction of the background magnetic field. Image from *Morton et al.* [2012a].

overdense flux tube relative to the ambient plasma. Models of this type in flux tube (i.e., cylindrical) geometry have been around since the late 1970s [e.g., *Zaitsev and Stepanov*, 1975; *Wentzel*, 1979; *Wilson*, 1979, 1980; *Edwin and Roberts*, 1983]. Deriving the dispersion relations in such models requires the physical constraints that the total pressure perturbations and normal velocity components be continuous at the flux tube boundary. This was a worthwhile advance on Alfvén's simple model, since it allowed for more realistic geometry and the possibility of both transverse magnetic field and plasma density inhomogeneities. The derived dispersion relations resulted in a much richer variety of MHD wave modes than was possible in Alfvén's more simple model. Assuming that the equilibrium plasma variation in the azimuthal direction of the flux tube is negligible, it allows for Fourier decomposition in that direction, and ultimately wave mode categorization in terms of the integer azimuthal wave number, m. For a cylindrical flux tube, the lowest order azimuthal wavenumber ($m = 0$) results in two distinct decoupled MHD axisymmetric wave modes, namely the incompressible torsional Alfvén [e.g., see *Hollweg*, 1978] and the compressible sausage [e.g., see *Nakariakov et al.*, 2003; *Aschwanden et al.*, 2004] modes. Their specific defining physical properties and their recent identification in chromospheric observations are discussed in Sections 25.3 and 25.4.

After $m = 0$, the next integer azimuthal wavenumber is $m = 1$, and this is associated with the so-called kink mode, which is the particular MHD wave mode under discussion in this section. As shown in Figure 25.2b, the key feature of this $m = 1$ mode is that it is the only value of m that produces a bulk transverse displacement of the flux tube. The $m = 0$ and all higher order ($m \geq 2$) fluting modes do not do this. Because of the plasma structuring the kink speed depends on both the internal magnetic field strength (B_i) and plasma density (ρ_i), as well as the external magnetic field strength (B_e) and plasma density (ρ_e). In the zero plasma-β limit equilibrium demands $B_e = B_i$. In this magnetically dominated plasma regime the kink speed, c_k, is described in the thin tube (or long wavelength) limit as

$$c_k = B\sqrt{\frac{2}{\mu(\rho_i + \rho_e)}} \tag{25.2}$$

where $B = B_e = B_i$. Note that the value of the kink speed lies between that of the internal and external Alfvén

speeds. The kink mode is highly Alfvénic since its main restoring force is magnetic tension (see the discussion by *Goossens et al*. [2009]). As discussed by *Van Doorsselaere et al*. [2008], it is also only weakly compressible in the long wavelength regime; hence it is unlikely that intensity perturbations due to compression/rarefaction could be readily observed for such waves. Actually *De Pontieu et al*. [2007] did not report any intensity perturbations concurrent with the transverse waves observed in spicules. Therefore, if present, they must be very small relative to the background intensity. So it is worthwhile to note that the absence of detectable intensity perturbations cannot be used as an argument to discount the presence of kink waves in favour of bulk Alfvén waves. *Erdélyi and Fedun* [2007] and *Van Doorsselaere et al*. [2008] also criticized the Alfvén wave interpretation of *De Pontieu et al*. [2007] from the flux tube perspective. Since Alfvén waves must be torsional in flux tube geometry, they would not display the bulk transverse motions observed in the imaging data of Figure 25.1; that is, the flux tube would appear stationary. This was the main argument put forward to support the kink-mode interpretation over the initial Alfvén wave interpretation suggested by *De Pontieu et al*. [2007].

Regarding observed properties of kink waves in spicules, in a case study of 94 events, *De Pontieu et al*. [2007] reported periods of 100–500 s and transverse velocity amplitudes on the order of $10-25\,\mathrm{kms}^{-1}$. A subsequent, but more limited case study by *He et al*. [2009a], also with Hinode/SOT data, reported the presence of higher frequency kink waves with periods as short as 40–50 s but with similar velocity amplitudes to that estimated by *De Pontieu et al*. [2007]. An advance on the work of *De Pontieu et al*. [2007] by *He et al*. [2009a] was an attempt to actually measure the upward propagation speed of the waves, resulting in values between $60-150\,\mathrm{kms}^{-1}$ up to 7 Mm above the solar limb. A larger case study of 89 spicules by *Okamoto and De Pontieu* [2011] found a median period of 45 s, which is more consistent with the period estimates of *He et al*. [2009a] than *De Pontieu et al*. [2007]. Interestingly, *Okamoto and De Pontieu* [2011] also reported that 59% of the waves were propagating upward, 21% propagating downward, and 20% standing. *Okamoto and De Pontieu* [2011] also estimated propagation speeds of $164-267\,\mathrm{kms}^{-1}$ up to 7 Mm above the limb but stated that inferred speeds greater than $1000\,\mathrm{kms}^{-1}$ above 10 Mm could not be physical. A possible explanation of this is that spicule intensity in chromospheric lines is too diffuse at higher altitudes to be reliable enough for wave studies.

Concerning another important class of chromospheric fine-scale magnetic structures, statistical studies of kink waves in fibrils have been made in a series of papers by *Morton et al*. [2012a, 2013, 2014]. Fibrils are low-lying elongated structures, most clearly seen on disc, that span supergranular cells [*Foukal*, 1971; *Zirin*, 1972]. Like spicules, they too have narrow widths ($\lesssim 1000\,\mathrm{km}$) and therefore need the highest resolution instruments available to analyze their wave properties. To this end, a range of statistical studies were performed by *Morton et al*. [2012a] to exploit the fantastic capabilities of ROSA [*Jess et al*., 2012a] equipped with a narrowband (0.25 Å) H α filter. *Morton et al*. [2012a] found that bulk transverse oscillations in fibrils, as in spicules, were omnipresent. It was reasoned that because fibrils appear dark in the line core of H α, it was most likely a result of a density enhancement relative to the ambient plasma that causes the radiative emission from the photosphere to suffer increased dimming in their vicinity [*Pietarila et al*., 2011]. Hence *Morton et al*. [2012a] classed fibrils as overdense waveguides and stated that their bulk transverse oscillations must, along with spicules, be interpreted as kink waves, not Alfvén waves. The combined studies of *Morton et al*. [2012a, 2013, 2014] analyzed 1688 fibril kink wave events in both the quiet Sun and active region chromospheres. The collated results gave most kink wave periods in the range of 94–130 s with velocity amplitudes of $5-25\,\mathrm{kms}^{-1}$, which are certainly of the same order as that found in the aforementioned observations of kink waves in spicules. Perhaps this should be expected, since both structures are rooted in intergranular lanes where it is likely they are excited by similar/identical drivers.

Kink waves on-disc have also been detected in mottles and via rapid blue-shifted excursions observed in the blue wings of chromospheric spectral lines. Apart from their wave properties, mottles and rapid blue-shifted excursions are of particular interest to solar physicists because it is thought they may be related directly (or indirectly) to spicules. Mottels, like spicules and fibrils, are also thin magnetically aligned structures less than 1000 km wide, but can either appear dark or bright in chromospheric lines. They were identified in scientific literature as far back as the early 1970s [e.g., *Alissandrakis and Macris*, 1971; *Sawyer*, 1972]. ROSA investigations of kink waves in mottles by *Kuridze et al*. [2012, 2013] revealed transverse velocity amplitudes on the order of $8-11\,\mathrm{kms}^{-1}$, which again are of the same order as found in spicules. The same is also true of kink waves detected in rapid blue-shifted excursions in large-scale statistical studies by *Rouppe van der Voort et al*. [2009] and *Sekse et al*. [2012, 2013], where they found transverse velocity amplitudes in a similar range. The observational characteristics of kink waves in all the various chromospheric waveguides discussed in this section are summarized in Table 25.1.

Table 25.1 Average (or individually measured) properties of chromospheric MHD kink waves.

Structure	Region	Max. Displacement Amplitude (km)	Period (s)	Max. Velocity Amplitude (kms^{-1})	Kink Speed (kms^{-1})	No. Events	Reference
Spicule	CH	200 – 500	150–350	20 ± 5	–	95	*De Pontieu et al.* [2007]
	CH	–	60–240	20 ± 5	–	–	*Suematsu et al.* [2008]
	CH	1000	130	15	460	1	*Kim et al.* [2008]
		700	180	8	310	1	
		800	170	9	260	1	
	CH	36	48	4.7	75 – 150	1	*He et al.* [2009a]
		36	37	6.1	59 – 117	1	
		130	45	18.1	73	1	
		166	50	20.8	109 – 145	1	
	CH	55 ± 50	45 ± 30	7.4 + 3.7	160 – 305	89	*Okamoto* and *De Pontieu* [2011]
		600	180	22	–	1	*Ebadi et al.* [2012]
	QS	670	220	19.2	–	1	*Jess et al.* [2012]
		630	139	28.3	–	1	
		160	65	14.8	–	1	
		410	158	16.2	–	1	
		380	129	18.5	–	1	
		200	105	11.8	–	1	
		190	171	7.2	–	1	
	AR	283 ± 218	–	14 ± 112	–	112	Type-I -*Pereira et al.* [2012]
	AR	463 ± 402	–	18 ± 12	–	58	Type-II
	QS	245 ± 211	–	16 ± 11	–	174	
	CH	342 ± 257	–	20 ± 12	–	170	
Fibrils		135	135	1	190	1	*Pietarila et al.* [2011]
	QS	315 ± 130	–	6.4 ± 2.8	50 – 90	103	*Morton et al.* [2012a]
	QS	71 ± 37	94 ± 61	24.5 ± 1.8	–		*Morton et al.* [2013]
	QS	94 ± 47	116 ± 59	5.5 ± 2.4	–	841	*Morton et al.* [2014]
	AR	73 ± 36	130 ± 92	4.4 ± 2.4	–	744	
Rapid blue-shifted		300	–	8	–	35	*Rouppe van der Voort et al.* [2009]
Excursions	CH	200	–	4 – 5	–	960	*Sekse et al.* [2012]
	QS	200	–	8.5	–	1951	Average *Sekse et al.* [2013]
		220	–	11.7	–	1951	Maximum
Mottles	QS	200 ± 67	165 ± 51	8.0 ± 3.6	–	42	*Kuridze et al.* [2012]
	QS	~172	$TE(=TE_i + TE_e)$	~9	50	1	*Kuridze et al.* [2013]
	QS	252	180 ± 10	8.8 ± 31	101 ± 14	1	
	QS	327	180 ± 10	11.4 ± 3.3	79 ± 8	1	

25.3. MHD SAUSAGE MODE IDENTIFICATION

Unlike the weakly compressible non-axisymmetric kink mode, the axisymmetric sausage mode is highly compressible, producing periodic changes to the cross-sectional area of a magnetic flux tube, analogous to fluid motion driven in an elastic tube by a peristaltic pump, as shown in Figure 25.7a. The presence of such motion was first detected in the Sun's lower atmosphere at the photospheric level in solar pores by *Dorotovič et al*. [2008] employing the G-band filter of the SST, and subsequently by *Fujimura and Tsuneta* [2009] and using Hinode/SOT. These intense magnetic features are essentially like small sunspots without penumbrae. Employing ROSA G-band data, *Morton et al*. [2011] accurately measured the periodic area and intensity changes exhibited by solar pores. It was found that some pores exhibited a clear anti-phase behavior between area and intensity oscillations that was strongly indicative of the sausage mode. For further and more in-depth discussions of photospheric sausage-mode observations, see Chapter 26. In the context of the present chapter, these initial photospheric discoveries naturally led to the search for sausage modes higher up in the chromosphere. Using ROSA H α data, *Morton et al*. [2012a] did indeed detect the anti-phase behavior of flux tube width changes and intensities in fibrils (see Figure 25.3). Furthermore these sausage waves were found to be concurrent with kink waves (whose identification in fibrils was previously discussed in Section 25.2). *Morton et al*. [2012a] found the sausage waves to have periods in the range 135–241 s and transversal velocities on the order of $1-2\,\mathrm{kms}^{-1}$. The resulting comparisons that can be made between kink/sausage energy fluxes in fibrils will be discussed in Section 25.5.

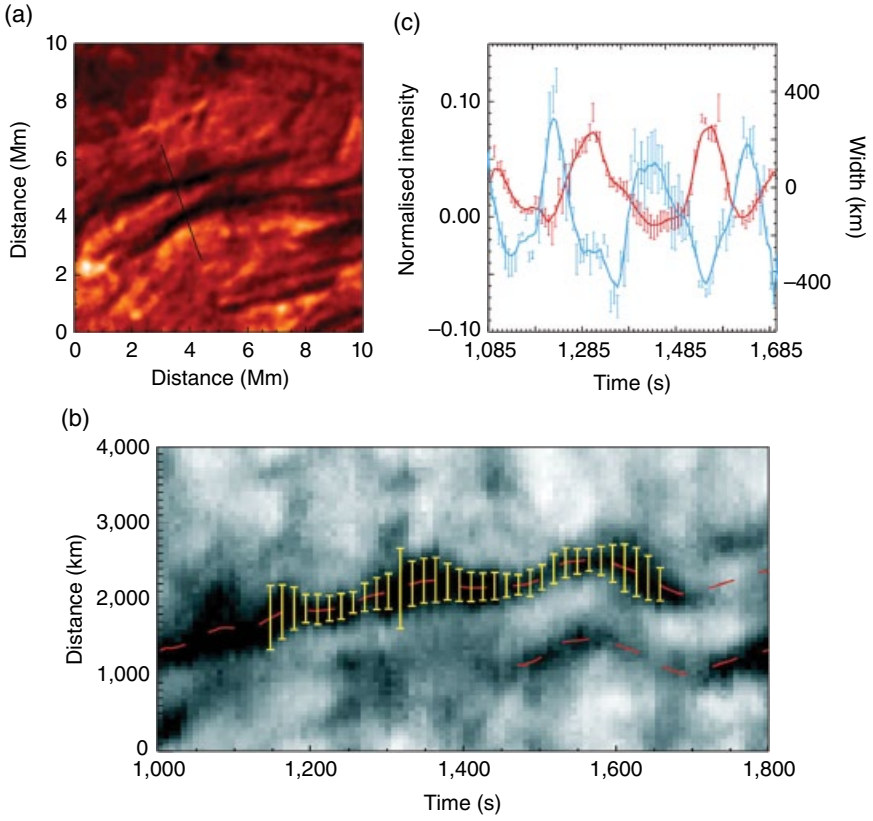

Figure 25.3 (a) Cropped ROSA H α snapshot containing a pair of dark, and hence dense, chromospheric flux tubes. (b) Cross-cut (black line) extracted intensity information, with the resulting time–distance diagram revealing the dynamic motion of the waveguides. Times are given in seconds from the start of the data set; the overplots are the results from a Gaussian fitting routine to show concurrent kink (red line shows the central axis of the structure) and sausage waves (yellow bars show the measured width of structure). The counterpropagating kink waves here have periods of 232 ± 8 s and phase speeds of $71 \pm 22\,\mathrm{kms}^{-1}$ upward and $87 \pm 26\,\mathrm{kms}^{-1}$ downward. The maximum transverse velocity amplitudes in both cases is about $5\,\mathrm{kms}^{-1}$. The sausage wave has a period of 197 ± 8 s, a phase speed of $67 \pm 15\,\mathrm{kms}^{-1}$, and a maximum transverse velocity amplitude of $1-2\,\mathrm{kms}^{-1}$. (c) Comparison between the detected intensity (blue) and width (red) perturbations resulting from the Gaussian fitting. Sausage waves can naturally cause such anti-phase behavior. Image reproduced from *Morton et al*. [2012a].

Slightly earlier work by *Jess et al*. [2012], again with ROSA H α data, actually detected similar joint kink- and sausage-mode signatures in spicules seen on-disc. However, *Jess et al*. [2012] did not explicitly associate the observed patterns as being concurrent sausage/kink waves. The authors were primarily concerned with the foot point driving mechanisms of these chromospheric waves since their dataset had simultaneous photospheric (G-band) and lower chromospheric (Ca II K) image sequences. G-band photospheric intensity oscillations showed a distinct phase difference of about 90° across a magnetic bright point located at the footpoint of a group of chromospheric spicules. A 2D MHD simulation was performed by *Jess et al*. [2012] using a compressive field-aligned footpoint driver of maximum amplitude 12.5 $\mathrm{km s^{-1}}$ combined with the observed spatial phase difference. This actually resulted in combined kink and sausage waves similar to those observed in spicules by *Jess et al*. [2012] and fibrils by *Morton et al*. [2012a]. Hence this could provide an explanation of why both highly and weakly compressive wave modes occur together in such fine-scale chromospheric structures. Thus far, sausage waves have not been detected in off-limb spicules. This could be due to complicated line-of-sight effects present in the "thick forest" of spicules seen off limb. However, for better understanding of spicule wave dynamics and energetics, proving their existence (or not) should certainly be the focus of future studies.

25.4. MHD TORSIONAL ALFVÉN WAVE IDENTIFICATION

Observations of small-scale photospheric vortical motions, detected via G-band bright point tracking in intergranular lanes, have been the subject of much interest in recent years [e.g., *Bonet et al*., 2008, 2010; *Wedemeyer-Böhm and Rouppe van der Voort*, 2009; *Steiner et al*., 2010; *Wedemeyer-Böhm et al*., 2012; *Morton et al*., 2013]. G-band bright points, of the order 200 km in diameter, are often cospatial with kG magnetic flux concentrations. In such cases they are often referred to as magnetic bright points [e.g., *Stenflo*, 1985; *Solanki*, 1993; *Crockett et al*., 2009; *Jess et al*., 2010b; *Keys et al*., 2011]. Such small-scale intense magnetic flux tubes rooted in vortex flow fields are natural sources of torsional Alfvén waves, as well as other MHD wave modes [e.g., *Fedun et al*., 2011a; *Shelyag et al*., 2013].

Torsional Alfvén waves, if propagating in a near or sub-resolution flux tube, could cause identifiable simultaneous periodic red and blue shifts in an observed spectral line. Since this process is not necessarily related to wave/energy dissipation inducing temperature fluctuations, it falls under the guise of periodic nonthermal spectral line broadening, providing the torsional amplitudes are large enough to cause noticeable red/blue shifts [*Zaqarashvili and Erdélyi*, 2009]. With H α data from the Solar Optical Universal Polarimeter (SOUP) based at the SST, *Jess et al*. [2009] detected such periodic spectral line broadening above a magnetic bright point group. Since there was an absence of both cospatial intensity oscillations and bulk transverse motions, the periodic spectral line broadening was interpreted by *Jess et al*. [2009] as evidence of torsional Alfvén waves. The estimated periods were in the range 126–700 s and the average line-of-sight velocity amplitude was approximately 1.5 $\mathrm{km s^{-1}}$.

Theoretically, torsional Alfvén waves can exist for any azimuthal wavenumber, m, and by definition, they are completely incompressible. A question that arises from interpreting observations as torsional Alfvén waves is: How likely is it that such purely divergence-free MHD wave modes are actually excited in the photosphere? Follow-up 3D MHD numerical investigations by *Fedun et al*. [2011b] of flux tubes driven by vortex drivers demonstrated that although torsional Alfvén waves could be the dominant wave mode, kink and sausage waves were still unavoidably present. This was because the chosen spiral driver did not have the particular azimuthal symmetry (or asymmetry) of one distinct m value but was a superposition of different m values. Feature-tracking studies to estimate horizontal velocity field components at vortex locations in the photosphere [e.g., *Morton et al*., 2013] show that this complicated scenario is actually much closer to reality.

Since spicules are rooted in intergranular lanes where such vortex motion occurs, it is natural to assume that torsional motion should be common in all of these structures. To search for this, the high-resolution capabilities of CRISP and the TRI-Port Polarimetric Echelle–Littrow (TRIPPEL) spectrograph, both based at the SST, were exploited by *De Pontieu et al*. [2012]. They were successful in actually resolving red-blue Doppler velocity asymmetries across the width of spicules in both H α and Ca II H data, interpreting this as the clear signature of torsional Alfvén waves (see Figure 25.4). Hence a more complete picture is now emerging of spicule dynamics. These chromospheric and interface region magnetic structures support at least three distinct types of motion, namely field-aligned flows along with both kink and torsional waves [*Sekse et al*., 2013]. Modeling all these motions as independent, *De Pontieu et al*. [2012] estimated that the best fit to observed data via Monte-Carlo simulations required field-aligned flows of 50–100 $\mathrm{km s^{-1}}$, kink velocities of 15–20 $\mathrm{km s^{-1}}$ and torsional motions of 25–30 $\mathrm{km s^{-1}}$. A drawback of this forward model is that by assuming these motions are independent, it completely neglects the physical magneto-fluid behavior of the plasma. Realistically, these motions are coupled, and this connectivity should be taken into account when interpreting data.

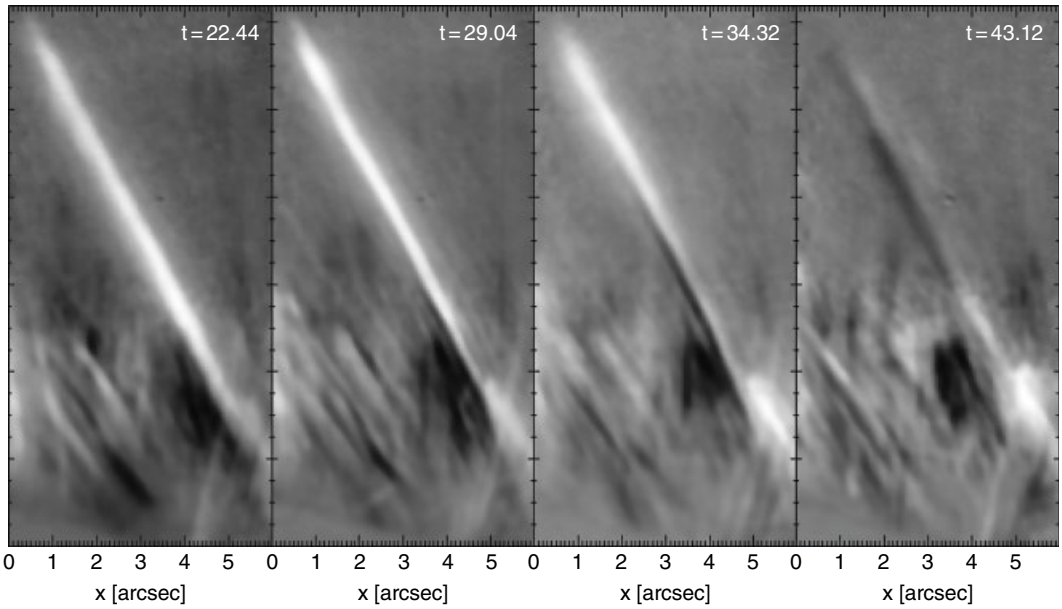

Figure 25.4 Sequences of four CRISP Hα Doppler images of a spicule at different sampling times (in seconds, blue-shift bright). The largest Doppler shifts in the spicule are approximately ±55 kms^{-1}. Image adapted from *De Pontieu et al*. [2012].

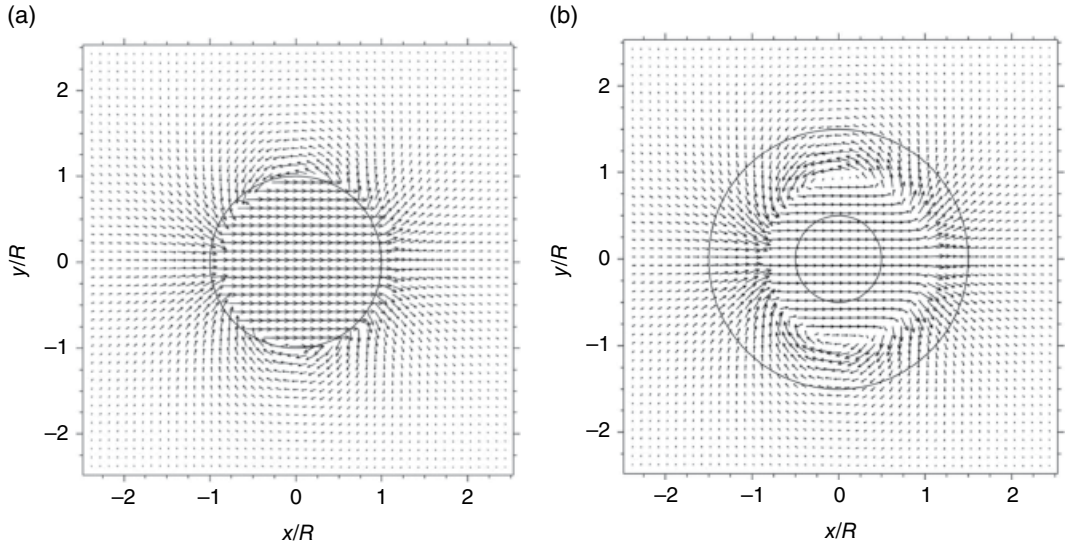

Figure 25.5 (a) Cross-cut of the kink wave displacement field (arrows), perpendicular to the flux tube axis. The internal and external densities are discontinuous at the boundary, indicated by the circle. (b) Kink "quasi-mode" displacement field (arrows) in a non-uniform tube with $l/R = 1$. The non-uniform density layer between the internal and external plasma is indicated by the annulus. The resultant resonance will cause the transverse motion of the kink wave to be mode converted into localized non-axisymmteric ($m = 1$) torsional Alfvén motion within the inhomogeneous layer, meaning the rotational motion will be amplified as the displacement field evolves. Image adapted from *Goossens et al*. [2014].

In the particular case of the $m = 1$ kink wave, it was pointed out by *Goossens et al*. [2014] that the velocity field of this MHD wave mode, even without the presence of other modes, is actually a combination of both transverse and rotational motion. Although in the long wavelength limit the internal velocity field is purely transversal, as shown in Figure 25.5a, the external field is dipolar in nature and could certainly contribute to rotational motion measured in observational data through artifacts of line-of-sight integration. Furthermore this rotational motion can be significantly enhanced for the kink wave through the process of resonant absorption shown in

Figure 25.5b. In essence, this mechanism causes the transverse energy of a kink wave to be channeled to the $m = 1$ torsional Alfvén wave in an inhomogeneous intermediate layer between the internal and external plasma where the kink wave frequency matches the local Alfvén frequency.

Unlike the $m = 0$ torsional Alfvén wave, the $m = 1$ torsional Alfvén wave does not have azimuthal symmetry [e.g., see *Spruit*, 1981] and would therefore not look the same to an observer from any given line-of-sight. *Goossens et al*. [2014] pointed out that the $m = 1$ rotational motions could produce very similar Doppler signatures to the $m = 0$ torsional Alfvén wave if the observer's line of sight is approximately perpendicular to the bulk transverse kink motion. Hence, if a spicule is observed to have a clear periodic transverse motion, indicating the presence of a kink wave, the Doppler signal across its width is likely to have a significant contribution from its $m = 1$ rotational motion. Although *De Pontieu et al*. [2011] mainly interpreted red/blue Doppler asymmetries as being due to the $m = 0$ torsional Alfvén wave, they did not discount the possibility of $m > 0$ rotational motion being present. This offers a great opportunity for both theorists and observers to understand the interplay between different MHD wave modes and flows in fine-scale chromospheric waveguides. To achieve this, the transverse structure should be spatially resolved, with simultaneous imaging and Doppler data combined to give an accurate insight into the true nature of the plasma dynamics at work.

So in summary, MHD wave mode identification in chromospheric waveguides has caused much and often heated debate. However, without this foundation knowledge, we cannot truly understand the various important aspects related to their contribution to the total energy budget of the solar atmosphere and their possible contribution to plasma heating. In this regard the following Section 25.5 reviews progress in determining more accurate energy flux estimations of specific MHD wave modes observed in the chromosphere.

25.5. MHD WAVE MODE ENERGY FLUX

As discussed in Section 25.2, *De Pontieu et al*. [2007] interpreted the transverse motions of spicules not as MHD kink waves, but as bulk Alfvén waves. This led them to also make energy flux estimates using the expression for such waves:

$$E = \frac{1}{2}\rho v^2 c_A \tag{25.3}$$

where v is the maximum transverse velocity amplitude and the factor 1/2 comes from the time-averaged energy over one complete period.

Equation (25.3) is only valid under the assumption of plasma homogeneity, which results in the equipartition between kinetic (KE) and magnetic (ME) energy. Furthermore *De Pontieu et al*. [2007] assumed that the energy associated with the transverse waves in spicules was of the same order elsewhere in the chromosphere and interface region, that is, in regions where transverse waves were not observable due to the intensity S/N ratio being too low. Hence *De Pontieu et al*. [2007] assumed the filling factor of the wave flux energy to be unity, even though spicules themselves are estimated to have a filling factor of no more than about 5% in the chromosphere [*Makita*, 2003; *Klimchuk*, 2012]. This has led to a number of serious criticisms by various authors [e.g., *Erdélyi and Fedun*, 2007; *Van Doorsselaere et al*., 2008, 2014; *Goossens et al*., 2013].

For the reasons discussed in Section 25.2, it was pointed out by *Erdélyi and Fedun* [2007] and *Van Doorsselaere et al*. [2008] that these transverse oscillations are more accurately interpreted as MHD kink waves. *Van Doorsselaere et al*. [2008] also went on to point out that kink wave energy flux would be strongly influenced by the filling factor of the plasma structure it was propagating through. For an overdense flux tube relative to the ambient plasma, as can be assumed for spicules, the kink wave energy flux takes in fact a maximum value within the tube itself and decays in the external region. The rate of decay depends on both the longitudinal wavenumber and density contrast. The larger the longitudinal wavenumber or density contrast, the faster the energy flux decays as a function of distance from the tube.

Importantly, *Goossens et al*. [2013] demonstrated that for $\rho_i \neq \rho_e$, a kink wave has no local equipartition of KE and ME. In the long wavelength approximation with $B_i = B_e$, the ratio of ME to KE inside the tube is

$$\left(\frac{\mathrm{ME}}{\mathrm{KE}}\right)_i = \frac{\rho_i + \rho_e}{2\rho_i} \tag{25.4}$$

and outside it is

$$\left(\frac{\mathrm{ME}}{\mathrm{KE}}\right)_e = \frac{\rho_i + \rho_e}{2\rho_e} \tag{25.5}$$

Also from *Goossens et al*. [2013], the ratio of external to internal total energy (TE = KE + ME) is

$$\frac{(\mathrm{TE})_e}{(\mathrm{TE})_i} = \frac{3\rho_e + \rho_i}{3\rho_i + \rho_e} \tag{25.6}$$

Equations (25.4) and (25.5) show that local energy equipartition is only possible if $\rho_e = \rho_i$. An overdense flux tube (i.e., $\rho_i > \rho_e$) results in $(\mathrm{ME/KE})_i < 1$ inside and $(\mathrm{ME/KE})_e > 1$ outside. Hence KE dominates inside the tube and ME dominates outside. Note also that $(\mathrm{TE})_e/(\mathrm{TE})_i < 1$, implying there is more of the total energy inside the tube than outside.

To illustrate the spatial variance in the distribution of energy with a specific numerical example, we take $\rho_i/\rho_e = 3$. This results in $(\mathrm{ME/KE})_i \approx 0.7$ and $(\mathrm{ME/KE})_e = 2$. The ratio of total energies gives $(\mathrm{TE})_e/(\mathrm{TE})_i = 0.6$; hence more than half the total energy is inside the tube. Denoting the flux tube radius as R, it can be shown that 90% of $\mathrm{TE}(=\mathrm{TE}_i + \mathrm{TE}_e)$ is within $2R$ of the flux tube axis, and 98.5% is within $5R$. Hence, even for a modest density ratio, $\rho_i/\rho_e = 3$, this still results in a notable localized concentration of energy in the immediate neighborhood of the flux tube. The larger the density ratio, the more localized this energy concentration will be. Therefore interpreting the transverse waves found in spicules as kink waves means that we have to take account of the spatially varying nature of the energy flux. *Van Doorsselaere et al*. [2014] derived an expression for the spatially averaged kink wave energy flux in a multi-tube system based on the calculations presented by *Goossens et al.* [2013], assuming small filling factors $(f \lesssim 0.1)$ as

$$E = \frac{1}{2} f \left(\rho_i + \rho_e\right) \upsilon^2 c_k \tag{25.7}$$

where all the quantities are assumed to be average values taken from kink waves propagating in a multi-flux tube system. In Equation (25.7), υ is the average kink wave maximum transverse velocity amplitude at the various locations of the dense flux tubes. Since for a kink wave the transverse velocity amplitude decays with distance from the flux tube, υ in Equation (25.7) has a physically distinct behavior to the maximum transverse velocity amplitude shown in Equation (25.3) for bulk Alfvén waves. In this simpler homogeneous plasma model, the Alfvén wave has a uniform velocity amplitude in space. Taking an upper bound spicule filling factor of $f = 0.05$, *Van Doorsselaere et al*. [2014] applied Equation (25.7) to the original bulk Alfvén wave energy flux estimates of *De Pontieu et al*. [2007] (derived using Equation 25.3), and found they were reduced from $4000 - 7000\,\mathrm{W\,m^{-2}}$ to $200 - 700\,\mathrm{W\,m^{-2}}$. This highlights the very important fact that if kink waves in an overdense solar waveguide are wrongly interpreted as bulk Alfvén waves, it can lead to a substantial overestimation of the energy flux. In the particular case of *De Pontieu et al*. [2007], the overestimation is believed to be at least an order of magnitude.

Regarding filling factors of fibrils seen on-disc, *Morton et al*. [2012a] estimated a comparable upper bound to spicules of 4–5%. For the energy flux estimate of kink waves in fibrils *Morton et al*. [2012a] only considered the energy inside the flux tubes, ignoring the external contribution. In essence, this is similar to what was done by *Van Doorsselaere et al*. [2014] in deriving Equation (25.7). Interestingly, *Morton et al*. [2012a] estimated the kink wave energy flux to be $170 \pm 110\ \mathrm{Wm^{-2}}$, the same order as that derived for spicules with the necessary filling factor correction by *Van Doorsselaere et al*. [2014]. This should not be surprising since spicules and fibrils both have similar densities, filling factors, and transverse wave amplitudes.

Incompressible wave energy flux in the different form of torsional Alfvén waves above a magnetic bright point group was estimated by *Jess et al*. [2009] to be about $240\,\mathrm{Wm^{-2}}$, assuming magnetic bright points cover at least 1.6% of the solar surface at any one time. This is of the same order as that estimated for filling factor corrected kink waves in fibrils and spicules. Again, this is not unexpected, since *Morton et al*. [2013] showed that photospheric vortex motion, which is the natural driver of torsional Alfvén waves, was also found to excite abundant chromospheric kink waves in H α fibrils.

Morton et al. [2012a] also estimated the sausage wave energy flux in fibrils to be on the order of $460 \pm 150\,\mathrm{Wm^{-2}}$, which is almost three times more than that found for kink waves, suggesting that compressive wave energy is more abundant than its incompressible counterpart. This has important implications for their ultimate fate, since compressive and incompressive MHD wave modes can have quite different physical damping mechanisms and rates, as discussed previously in Section 25.1.

Here we add the caveat that such energy flux estimates, filling factor arguments aside, are based on resolved wave amplitudes only. Therefore a substantial amount of wave energy may still be unaccounted for. In the corona, it has already been suggested by many authors [e.g., *Hassler et al*., 1990; *Hassler and Moran*, 1994; *Banerjee et al*., 1998], that measured nonthermal spectral line broadening between about 20 and $50\,\mathrm{kms^{-1}}$ could have a significant contribution from sub-resolution waves. With respect to the chromosphere, the soon to be operational Daniel K. Inouye Solar Telescope (DKIST) in Maui, with its 4 m diameter telescope, will offer a much improved tool to probe the smaller scale wave dynamics than is currently available (e.g., via the 1 m SST and the 0.76 m DST). To put this into perspective, the two-pixel diffraction-limited spatial resolution at Ca II K wavelengths obtained by the DKIST will be sub-20 km, compared with the near-100 km resolution offered by the DST. By helping us better understand the velocity fields and fine structure of chromosphere waves, it will also provide us with more accurate energy flux estimates.

In summary, it was to be expected that from the preceding debate about chromospheric MHD wave mode identification, arguments would also arise about the actual energy flux they contain. In this section, we have highlighted some of the main differing ideas on this contentious issue. In the next section, we go on to review how the discovery of these MHD wave modes has helped us advance the field of chromospheric magnetoseismology.

25.6. ADVANCES IN CHROMOSPHERIC MAGNETOSEISMOLOGY

Significantly, using Hinode/SOT Ca II H data, *He et al*. [2009b] measured the variation in both propagation speed and velocity amplitude of kink waves as they traveled along spicules. *Verth et al*. [2011] exploited this detailed information for the purpose of implementing chromospheric magnetoseismology. Previously magnetoseismology in the Sun's atmosphere was limited to TRACE observations of post-flare standing kink waves in coronal loops [e.g., *Nakariakov and Ofman*, 2001; *Aschwanden*, 2004]. Since it was mostly the fundamental mode that was observed in such events, this did not provide enough information for wave theorists to determine how the plasma density and magnetic field were varying along such structures. Obtaining more detailed information about field-aligned plasma inhomogeneity length scales from standing kink wave observations requires the detection of higher harmonics [e.g., see *Andries et al*., 2009], and unfortunately, these were found much less frequently in the data. However, after the discovery of ubiquitous propagating kink waves in the chromosphere, this opened a whole new avenue in solar atmospheric magnetoseismology. The governing kink wave equation that had initially been derived for standing kink waves in coronal loops of longitudinally varying magnetic field and plasma density [e.g., see *Ruderman et al*., 2008; *Andries and Cally*, 2011] could now be applied to observations of propagating waves in the lower atmosphere. The ordinary differential equation that describes the transverse velocity component of undamped kink waves in the thin tube regime is

$$\frac{d^2}{ds^2}\left(\frac{\upsilon}{R}\right)+\frac{w^2}{c_k^2(s)}\left(\frac{\upsilon}{R}\right)=0 \tag{25.8}$$

where s is the magnetic field aligned coordinate, ω is the angular frequency, $\upsilon(s)$ is the maximum transverse velocity component, $R(s)$ is the flux tube radius, and

$$c_k^2(s)=\frac{B^2(s)}{\mu\langle\rho(s)\rangle} \tag{25.9}$$

where $B(s)$ is the magnetic field strength, taken to be the same inside and outside the tube, and $\langle\rho_i(s)\rangle=[\rho_i(s)+\rho_e]/2$ is the average of the internal and external densities.

If both the maximum transverse velocity, $\upsilon(s)$, and kink speed, $c_k(s)$, are estimated from observations, then (25.8) can be solved for the only unknown, $R(s)$. From the determined $R(s)$ and the thin tube magnetic flux conservation relation

$$B(s)\propto\frac{1}{R^2(s)} \tag{25.10}$$

the variation in magnetic field, $B(s)$, along the flux tube can also be deduced. Combining $B(s)$ with the original observational estimate of $c_k(s)$, we can go back to (25.9) for determining the field aligned variation in average plasma density,

$$\langle\rho(s)\rangle\propto\frac{B^2(s)}{c_k^2(s)} \tag{25.11}$$

Therefore observational estimates of $\upsilon(s)$ and $c_k(s)$ allow us to determine the variation of both the magnetic field and plasma density along solar waveguides.

Verth et al. [2011] pioneered this magnetoseismological approach to find the variation of $R(s)$, $B(s)$, and $\langle\rho(s)\rangle$ along a spicule (see Figure 25.6). This technique was later implemented by *Kuridze et al*. [2013] and *Morton* [2014] in further investigations of mottles and spicules, respectively. In fine-scale plasma structures of near-resolution width such as spicules and mottles, $R(s)$ can be difficult to determine from intensity information alone [e.g., see *DeForest*, 2007]. Also traditional methods for determining plasma density and magnetic field strengths in the chromosphere through spectroscopy [e.g., *Makita*, 2003; *Bjølseth*, 2008] and polarimetry [e.g., *Trujillo Bueno et al*., 2005; *Centeno et al*., 2010] have their own inherent problems. Hence magnetoseismology provides a much needed complementary approach in determining near- (or even sub-) resolution structuring of the chromosphere.

Note that for Equation (25.8) the propagating wave envelope, $\upsilon(s)$, is independent of ω since the effect of frequency-dependent damping is not included. *Verth et al*. [2011] pointed out that if damping was present this would result in underestimating the rate of change of $R(s)$ and hence the other quantities, $B(s)$ and $\langle\rho(s)\rangle$. In fact the damping rate of kink waves and other MHD wave modes in the chromosphere are of much interest, but so far little is known. In contrast, the damping rates of post-flare/CME standing kink waves in the corona have been very well studied. In a statistical analysis of 52 standing kink wave events in coronal loops, using combined TRACE and SDO/AIA data, *Verwichte et al*. [2013] found most quality factors were in the range $\tau/P\approx1-4$, where τ is the damping time and P the period. A widely supported physical mechanism to explain this is resonant absorption (see the review by *Goossens et al*. [2011]). In an overdense flux tube resonant behavior is often modeled analytically by the inclusion of an annulus at the boundary where the value of density decreases continuously from ρ_i to ρ_e. Hence an Alfvén continuum is introduced into the flux tube via the creation of a boundary layer. Since the kink frequency is between that of the internal and external Alfvén frequencies, at some position in the boundary layer the kink frequency will match that of the local Alfvén frequency and a resonance will occur.

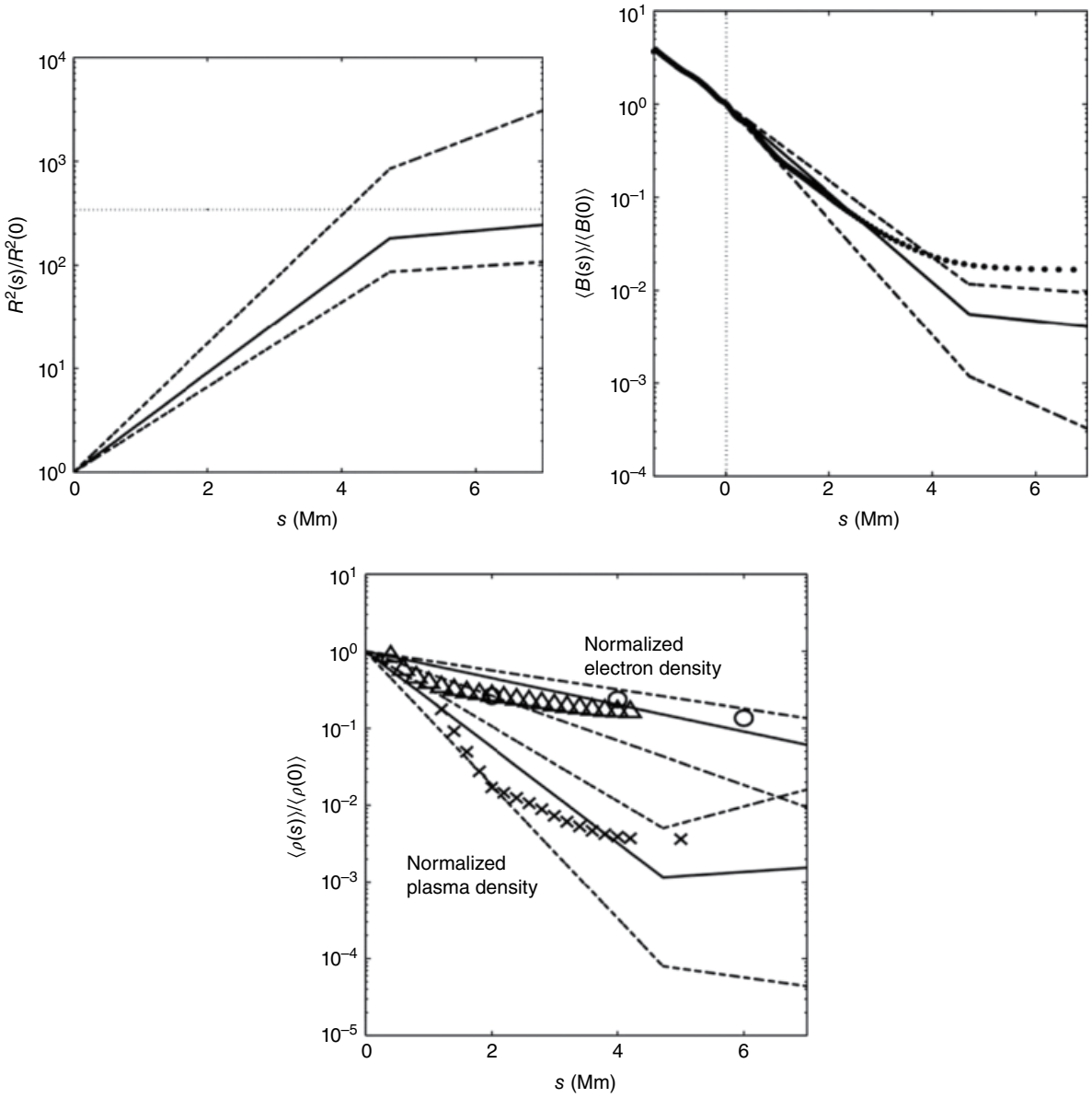

Figure 25.6 Magnetoseismically derived estimates of background variables along a spicule by *Verth et al*. [2011] compared with results of other authors. The left panel shows the estimated area expansion of the flux tube, normalized to unity at the spicule footpoint $s = 0$, where s is the field-aligned coordinate along the spicule. The dashed lines signify the 95% confidence bounds. The dotted horizontal line denotes the upper limit estimated by *Tsuneta et al*. [2008a] using Hinode/SOT data. The middle panel indicates the estimated decrease in magnetic field strength with height, normalized to unity at $s = 0$. The dashed lines also signify the 95% confidence bounds. The dots show the average unsigned magnetic field strength from the radiative MHD simulations of *De Pontieu et al*. [2007] to a depth of 1.4 Mm. The vertical dotted line indicates the position of the photosphere. The right panel illustrates both normalized plasma and electron density. The solid line indicates the magnetoseismically determined variation in plasma density from *Verth et al*. [2011], with the dashed lines indicating the 95% confidence bounds. The crosses are from Table 1 of *Makita* [2003]. Regarding the normalized electron density, the circles are from Table XIX of *Beckers* [1968] and the triangles are from Table 1 of *Makita* [2003]. The estimate and uncertainties by *Bjølseth* [2008] are shown by the solid and dashed lines respectively. Image adapted from *Verth et al*. [2011].

This causes the kink wave to be mode converted to the $m = 1$ torsional Alfvén wave in the boundary layer, resulting in the observed kink transverse motion becoming damped. Analytically, this process can be described most easily in the thin tube thin boundary (TTTB) approximation, which predicts an exponential kink wave damping rate with a quality factor

$$\frac{\tau}{P} = F \frac{R}{l} \frac{\rho_{\mathrm{i}} + \rho_{\mathrm{e}}}{\rho_{\mathrm{i}} - \rho_{\mathrm{e}}} \tag{25.12}$$

where l is the width of the inhomogeneous density layer, R is the flux tube radius, and the factor F depends on the functional form chosen for the decrease in density between ρ_i and ρ_e. To give a particular example, choosing a sinusoidal decrease results in $F = 2/\pi$. It can be seen from (25.12) that the damping time can be reduced by increasing the boundary layer width relative to the flux tube radius (larger l/R), and also by increasing the internal/external density contrast (larger ρ_i/ρ_e). The damping rate predicted by (25.12) has been exploited to determine the cross-field variation in plasma density in solar atmospheric waveguides through observed damping rates. Primarily, this has been attempted for standing and propagating kink waves in the corona [e.g., see *Aschwanden et al*., 2003; *Arregui et al*., 2007; *Verth et al*., 2010]. Now there is such an extensive data set for the damping rates of coronal kink waves, even more advanced statistical models are now being employed [e.g., *Arregui et al*., 2013; *Verwichte et al*., 2013; *Arregui and Asensio Ramos*, 2014]. In contrast, to date there have only been a few attempts at estimating the in situ damping rates of kink waves in the chromosphere [e.g., *Kuridze et al*., 2012; *Morton*, 2014].

The basis of support for the mechanism of resonant absorption to explain observed kink wave damping is mostly founded on two separate arguments. First, expected order-of-magnitude values for both viscosity and resistivity in the corona would not account for the reasonably fast damping rates [e.g., *Nakariakov et al*., 1999]. Second, flux tubes in the solar atmosphere are unlikely to have perfect discontinuities in Alfvén speed at their boundaries as idealized by *Edwin and Roberts* [1983]. Hence inclusion of a more realistic Alfvén continuum between the internal and external plasma would naturally introduce a resonant layer for the kink wave. For a broadband frequency driver, resonant absorption and the resultant process of mode conversion will cause m=1 torsional Alfvén waves to be excited on many magnetic surfaces, which will then phase mix. This may lead to Kelvin–Helmholtz instabilities between neighboring magnetic surfaces, which in turn will generate smaller length scales at which heating becomes more efficient [e.g., *Ofman et al*., 1998; *Terradas et al*., 2008; *Antolin et al*., 2014].

Importantly, such broadband frequency propagating kink waves were discovered in coronal loops with the CoMP instrument by *Tomczyk et al*. [2007]. This inspired theorists to model the process of resonant absorption for propagating kink waves. Initial work in this area was by *Terradas et al*. [2010], who found that the damping length (L_D) for kink waves in the TTTB approximation is inversely proportional to the frequency, f,

$$L_D = \frac{1}{f}\left(\frac{\tau}{P}\right) c_k \tag{25.13}$$

Hence the process of resonant damping of kink waves acts like a low-pass filter in solar atmospheric waveguides.

Verth et al. [2010] fitted Equation (25.13) to CoMP data of broadband frequency kink waves propagating in coronal loops with $c_k \approx 600\mathrm{kms}^{-1}$ and found $\tau / P \approx 2.7$, consistent with the range expected for standing kink waves ($\tau / P \approx 1-4$). Such frequency dependent damping should be detectable in velocity power spectra as a function of height in the solar atmosphere. In fact *Morton et al*. [2014] searched for this by comparing velocity power spectra from both the chromosphere and corona using the ROSA/DST and CoMP instruments, respectively. Interpolating over the height spanned by the interface region between the ROSA/DST and CoMP data (approximately 10–15 Mm), it was found that the damping length of kink waves in the interface region was about 12.5% of that previously estimated in the corona. This provided tentative evidence of greatly enhanced damping of propagating kink waves in the Sun's lower atmosphere. *Morton et al*. [2014] suggested that this could be caused by a combination of smaller quality factors and lower kink speeds in the interface region. The recently launched IRIS spacecraft, which is specifically designed to give the highest spatial/temporal resolution yet in interface region spectral lines, will be an invaluable tool to push forward from these initial studies by *Morton et al*. [2014] and actually measure the changing properties of kink waves as they traverse this fascinating region. Certainly, a whole new era of chromospheric and interface region magnetoseismology is opening up before us.

25.7. SUMMARY

Until the launch of Hinode in 2006, solar atmospheric MHD wave observers and theorists were almost exclusively focused on the corona. However, with the discovery of ubiquitous transverse waves in chromospheric and interface region spicules by *De Pontieu et al.* [2007], this branch of solar atmospheric wave research gained a whole new lease of life. Now there is vigorous debate about which particular MHD wave mode (or modes) are being observed in the Sun's lower atmosphere. Moreover this has naturally lead to intense discussions about how best to

quantify their associated energy flux, knowledge of which is crucial for understanding the contribution of waves to plasma heating. The plethora of high spatial/temporal ground- and space-based chromospheric imaging and spectroscopic data now available has also allowed the first magnetoseismic studies of this fascinating and complex region. This has proved an especially useful complementary tool to probe the fine-scale plasma structuring of the chromosphere. With the more traditional methods of spectroscopy and polarimetry, it is very difficult to estimate even average plasma densities and magnetic field strengths in near-resolution width and short-lived chromospheric features such as spicules, fibrils, and mottles, far less how they vary in time and space. Now magnetoseismology really has something to offer in this regard. In the context of all-encompassing studies of MHD wave propagation and energy deposition throughout the whole solar atmosphere, it is becoming increasingly clear that chromospheric waves play a vital role. In conclusion, a whole new era of chromospheric MHD wave research has truly unfolded, offering fantastic opportunities and challenges to both theorists and observers alike.

ACKNOWLEDGMENTS

G.V. acknowledges the support of the Leverhulme Trust (UK). D.B.J. wishes to thank the UK Science and Technology Facilities Council (STFC) for the award of an Ernest Rutherford Fellowship alongside a dedicated Research Grant. The authors also acknowledge R. J. Morton for collating the data used in Table 25.1.

REFERENCES

Alissandrakis, C. E., and Macris, C. J. (1971), *Sol. Phys.*, *20*, 47.
Alfvén, H. (1942), *Nature*, *150*, 405.
Andries, J. and Cally, P. S. (2011), *Astrophys. J.*, *743*, 164.
Andries, J., Van Doorsselaere, T., Roberts, B., et al. (2009), *Space Sci. Rev.*, *149*, 3.
Antolin, P., Yokoyama, T., and Van Doorsselaere, T. (2014), *Astrophys. J.*, *787*, L22.
Arregui, I., Andries, J., Van Doorsselaere, T., Goossens, M., and Poedts, S. (2007), *Astron. Astrophys.*, *463*, 333.
Arregui, I. and Asensio Ramos, A. (2014), *Astron. Astrophys.*, *565*, 78.
Arregui, I., Asensio Ramos, A., and Pascoe, D. J. (2013), *Astrophys. J.*, *769*, L34.
Aschwanden, M. J. (2004), *Physics of the Solar Corona: An Introduction* (Chichester: Praxis).
Aschwanden, M. J., Nakariakov, V. M., and Melnikov, V. F. (2004), *Astron. Astrophys.*, *600*, 458.
Aschwanden, M. J., Nightingale, R. W., Andries, J., Goossens, M., and Van Doorsselaere, T. (2003), *Astrophys. J.*, *598*, 1375.
Banerjee, D., Teriaca, L., Doyle, J. G., et al. (1998), *Astron. Astrophys.*, *339*, 208.
Beckers, J. M. (1968), *Sol. Phys.*, *3*, 367.
Bjølseth, S. (2008), Masters Spicules, Univ. Oslo.
Bonet, J. A., Màrquez, I., Sànchez Almeida, J., Cabello, I., and Domingo, V. (2008), *Astrophys. J., 687*, L131.
Bonet, J. A., Màrquez, I., Sànchez Almeida, J., et al. (2010), *Astrophys. J.*, *723*, L139.
Centeno, R., Trujillo Bueno, J., and Asensio Ramos, A. (2010), *Astrophys. J.*, *708*, 1579.
Crockett, P. J., Jess, D. B., Mathioudakis, M., and Keenan, F. P. (2009), *Mon. Not. R. Astron. Soc.*, *397*, 1852.
DeForest, C. E. (2007), *Astrophys. J.*, *661*, 532.
De Pontieu, B., Carlsson, M., Rouppe van der Voort, L. H. M., et al. (2012), *Astrophys. J.*, *752*, L12.
De Pontieu, B., McIntosh, S. W., Carlsson, M., et al. (2007), *Science*, *318*, 1574.
De Pontieu, B., McIntosh, S. W., Carlsson, M., et al. (2011), *Science*, *331*, 55.
De Pontieu, B., Title, A. M., Lemen, J. R., et al. (2014), *Sol. Phys.*, *289*, 2733.
Domingo, V., Fleck, B., and Poland, A. I. (1995), *Space Sci. Rev.*, *72*, 81.
Ebadi, H., Zaqarashvili, T. V. and Zhelyazkov, I. (2012), *Astrophys. and Space Sci.*, *337*, 33.
Edwin, P. M., and Roberts, B. (1983), *Sol. Phys.*, *88*, 179.
Erdélyi, R., and Fedun, V. (2007), *Science*, *318*, 1572.
Fedun, V., Shelyag, S., Verth, G., Mathioudakis, M. and Erdélyi, R. (2007a), *Ann. Geophys.*, *29*, 1029.
Fedun, V., Verth, G., Jess, D. B., and Erdélyi, R. (2011b), *Astrophys. J.*, *740*, L46.
Foukal, P. (1971), *Sol. Phys.*, *20*, 298.
Fujimura, D., and Tsuneta, S. (2009), *Astrophys. J., 702*, 1443.
Goossens, M., Erdélyi, R., and Ruderman, M. R. (2011), *Space Sci. Rev.*, *158*, 289.
Goossens, M., Soler, R., Terradas, J., Van Doorsselaere, T. and Verth, G. (2014), *Astrophys. J.*, *788*, 9.
Goossens, M., Terradas, J., Andries, J., Arregui, I., and Ballester, J. L. (2009), *Astron. Astrophys.*, *503*, 213.
Goossens, M., Van Doorsselaere, T., Soler, R., and Verth, G. (2013), *Astrophys. J.*, *768*, 191.
Handy, B. N., Acton, L. W., Kankelborg, C. C., et al. (1999), *Sol. Phys.*, *187*, 229.
Hansteen, V. H., Carlsson, M., and Gudiksen, B. (2007), in *ASP Conf. Ser. 368, The Physics of Chromospheric Plasmas*, edited by P. Heinzel, I. Dorotovic, and R. J. Rutten (San Francisco, CA: ASP), *107*.
Hassler, D. M., and Moran, T. G. (1994), *Space Sci. Rev.*, *70*, 373.
Hassler, D. M., Rottman, G. J., Shoub, E. C., and Holzer, T. E. (1990), *Astrophys. J.*, *348*, L77.
He, J.-S., Marsch, E., Tu, C.-Y., and Tian, H. (2009a), *Astrophys. J.*, *705*, 217.
He, J.-S., Tu, C.-Y., Marsch, E., et al. (2009b), *Astron. Astrophys.*, *497*, 525.
Hollweg, J.V. (1978), *Sol. Phys.*, *56*, 305.
Judge, P. (2006), in *ASP Conf. Ser. 354, Solar MHD Theory and Observations: A High Spatial Resolution Perspective*, edited by J. Leibacher, R. F. Stein, and H. Uitenbroek (San Francisco, CA: ASP), 259.
Jess, D. B., Mathioudakis, M., Christian, D. J., et al. (2010a), *Sol. Phys.*, *261*, 363.

Jess, D. B., Mathioudakis, M., Christian, D. J., Crockett, P. J. and Keenan, F. P. (2010b), *Astrophys. J.*, *719*, L134.
Jess, D. B., Mathioudakis, M., Erdélyi, R., et al. (2009), *Science*, *323*, 1582.
Jess, D. B., Morton, R. J., Verth, G., et al. (2015), *Space Sci. Rev.*, DOI: 10.1007/s11214-015-0141-3.
Jess, D. B., Pascoe, D. J., Christian, D. J., et al. (2012), *Astrophys. J.*, *744*, L5.
Keys, P. H., Mathioudakis, M., Jess, D. B, et al. (2011), *Astrophys. J.*, *740*, L40.
Kim, Y.-H, Bong, S.-C., Park, Y.-D., et al. (2008), *J. Korean Astron. Soc.*, *41*, 173.
Klimchuk, J. A. (2012), *J. Geophys. Res. (Space Phys.)*, *117*, 12102.
Kosugi, T., Matsuzaki, K., Sakao, T., et al. (2007), *Sol. Phys.*, *243*, 3.
Kukhianidze, V., Zaqarashvili, T. V., and Khutsishvili, E. (2006), *Astron. Astrophys.*, *449*, L35.
Kuridze, D., Morton, R. J., Erdélyi, R., et al. (2012), *Astron. Astrophys.*, *750*, 51.
Kuridze, D., Verth, G., Mathioudakis, M., et al. (2013), *Astron. Astrophys.*, *779*, 82.
Lemen, J. R., Title, A. M., Akin, D. J., et al. (2012), *Sol. Phys.*, *275*, 17.
Makita, M. (2003), *Pub. Nat. Astron. Obs. Japan*, *7*, 1.
Martínez-Sykora, J., De Pontieu, B., Leenaarts, J., et al. (2013), *Astron. Astrophys.*, *771*, 66.
Martínez-Sykora, J., Hansteen, V., and Moreno-Insertis, F. (2011), *Astrophys. 736*, 9
Morton, R. J. (2014), *Astron. Astrophys.*, *566*, 90.
Morton, R. J., Erdélyi, R., Jess, D. B. and Mathioudakis, M. (2011), *Astrophys. J.*, *729*, L18.
Morton, R. J., Verth, G., Fedun, V., Shelyag, S., and Erdélyi, R. (2013), *Astrophys., J*, *768*, 17.
Morton, R. J., Verth, G., Hillier, A., and Erdélyi, R. (2014), *Astrophys. J.*, *784*, 29.
Morton, R. J., Verth, G., Jess, D. B., et al. (2012a), *Nature Comm.*, *3*.
Morton, R. J., Verth, G., McLaughlin, J. A. and Erdélyi, R. (2012b), *Astrophys. J.*, *744*, 5.
Nakariakov, V. M., Melnikov, V. F., and Reznikova, V. E. (2003), *Astron. Astrophys.*, *412*, L7.
Nakariakov, V. M., and Ofman, L. (2001), *Astron. Astrophys.*, *372*, L53.
Nakariakov, V. M., Ofman, L., DeLuca, E. E., Roberts, B., and Davila, J. M. (1999), *Science*, *285*, 862.
Nikol'Sky, G. M., and Sazanov, A. A. (1967), *Sov. Astron.*, *10*, 744.
Ofman, L., Klimchuk, J. A., and Davila, J. M. (1998), *Astrophys. J.*, *493*, 474.
Okamoto, T. J., and De Pontieu, B. (2011), *Astrophys. J.*, *736*, L24.
Pasachoff, J. M., Noyes, R. W., and Beckers, J. M. (1968), *Sol. Phys. 5*, 131.
Pereira, T. M. D., De Pontieu, B., and Carlsson, M. (2012), *Astrophys. J.*, *759*, 18.
Pietarila, A., Aznar Cuadrado, R., Hirzberger, J., and Solanki, S. K. (2011), *Astrophys. J.*, *739*, 92.
Rouppe van der Voort, L., Leenaarts, J., De Pontieu, B., Carlsson, M., and Vissers, G. (2009), *Astrophys. J.*, *705*, 272.
Ruderman, M. S., Verth, G., and Erdélyi, R. (2008), *Astrophys. J.*, *686*, 694
Sawyer, C. (1972), *Sol. Phys.*, *24*, 79.
Scharmer, G. B., Narayan, G., Hillberg, T., et al. (2008), *Astrophys. J.*, *689*, L69.
Secchi, P. A. (1877), *Le Soleil*, Vol. *2* (Paris: Gauthier-villas).
Sekse, D. H., Rouppe van der Voort, L. and De Pontieu, B. (2012), *Astrophys. J.*, *752*, 108.
Sekse, D. H., Rouppe van der Voort, L., De Pontieu, B. and Scullion, E. (2013), *Astrophys. J.*, *769*, 44.
Shelyag, S., Cally, P. S., Reid, A., and Mathioudakis, M. (2013), *Astrophys. J.*, *776*, L4.
Solanki, S. K. (1993), *Space Sci. Rev.*, *63*, 1.
Spruit, H. C. (1981), *Sol. Phys.*, *75*, 3.
Steiner, O., Franz, M., Bello Gonzàlez, N., et al. (2010), *Astrophys. J.*, *723*, L180.
Stenflo, J. O. (1985), *Sol. Phys.*, *100*, 189.
Suematsu, Y., Ichimoto, K., Katsukawa, Y., et al. (2008), in *ASP Conf. Ser. 397, First Results from Hinode*, edited by S. A. Matthews, J. M. Davis, and L. K. Harra (San Francisco, CA: ASP), 27.
Suematsu, Y., Tsuneta, S., Ichimoto, K., et al. (2008), *Sol. Phys.*, *249*, 197.
Terradas, J., Andries, J., Goossens, M., et al. (2008), *Astrophys. J.*, *687*, L115.
Terradas, J., Goossens, M., and Verth, G. (2010), *Astron. Astrophys.*, *524*, 23.
Tomczyk, S., and McIntosh, S. W. (2009), *Astrophys. J.*, *697*, 1384.
Tomczyk, S., McIntosh, S. W., Keil, S. L. et al. (2007), *Science*, *317*, 1192.
Trujillo Bueno, J., Merenda, L., Centeno, R., Collados, M., and Landi DeglInnocenti, E. (2005), *Astrophys. J.*, *619*, L191.
Tsuneta, S., Ichimoto, K., Katsukawa, Y. et al. (2008a), *Astrophys. J.*, *688*, 1374.
Tsuneta, S., Ichimoto, K., Katsukawa, Y., et al. (2008b), *Sol. Phys.*, *249*, 167.
Van Doorsselaere, T., Gijsen, S. E., Andries, J. and Verth, G. (2014), *Astrophys. J.*, *795*, 18.
Van Doorsselaere, T., Nakariakov, V. M., and Verwichte, E. (2008), *Astrophys. J.*, *676*, 73.
Verth, G., Goossens, M. and He, J.-S. (2011), *Astrophys. J.*, *733*, 15.
Verth, G., Terradas, J. and Goossens, M. (2010), *Astrophys. J.*, *718*, L102.
Verwichte, E., Van Doorsselaere, T., White, R. S. and Antolin, P. (2013), *Astron. Astrophys.*, *552*, 138.
Weart, S. R. (1970), *Sol. Phys.*, *14*, 310.
Wedemeyer-Böhm, S., and Rouppe van der Voort, L. (2009), *Astron. Astrophys.*, *507*, L9.
Wedemeyer-Böhm, S., Scullion, E., Steiner, O., et al. (2012), *Nature*, *486*, 505.
Wentzel, D. G. (1979), *Astron. Astrophys.*, *76*, 20.
Wilson, P. R. (1979), *Astron. Astrophys.*, *71*, 9.
Wilson, P. R. (1980), *Astron. Astrophys.*, *87*, 121.
Zaqarashvili, T. V., and Erdélyi, R. (2009), *Space Sci. Rev.*, *149*, 355.
Zaitsev, V. V., and Stepanov, A. V. (1975), *Issled. Geomagn. Aeron. Fiz. Solntsa*, *37*, 3.
Zirin, H. (1972), *Sol. Phys.*, *22*, 34.